

# Soft Matter

Accepted Manuscript

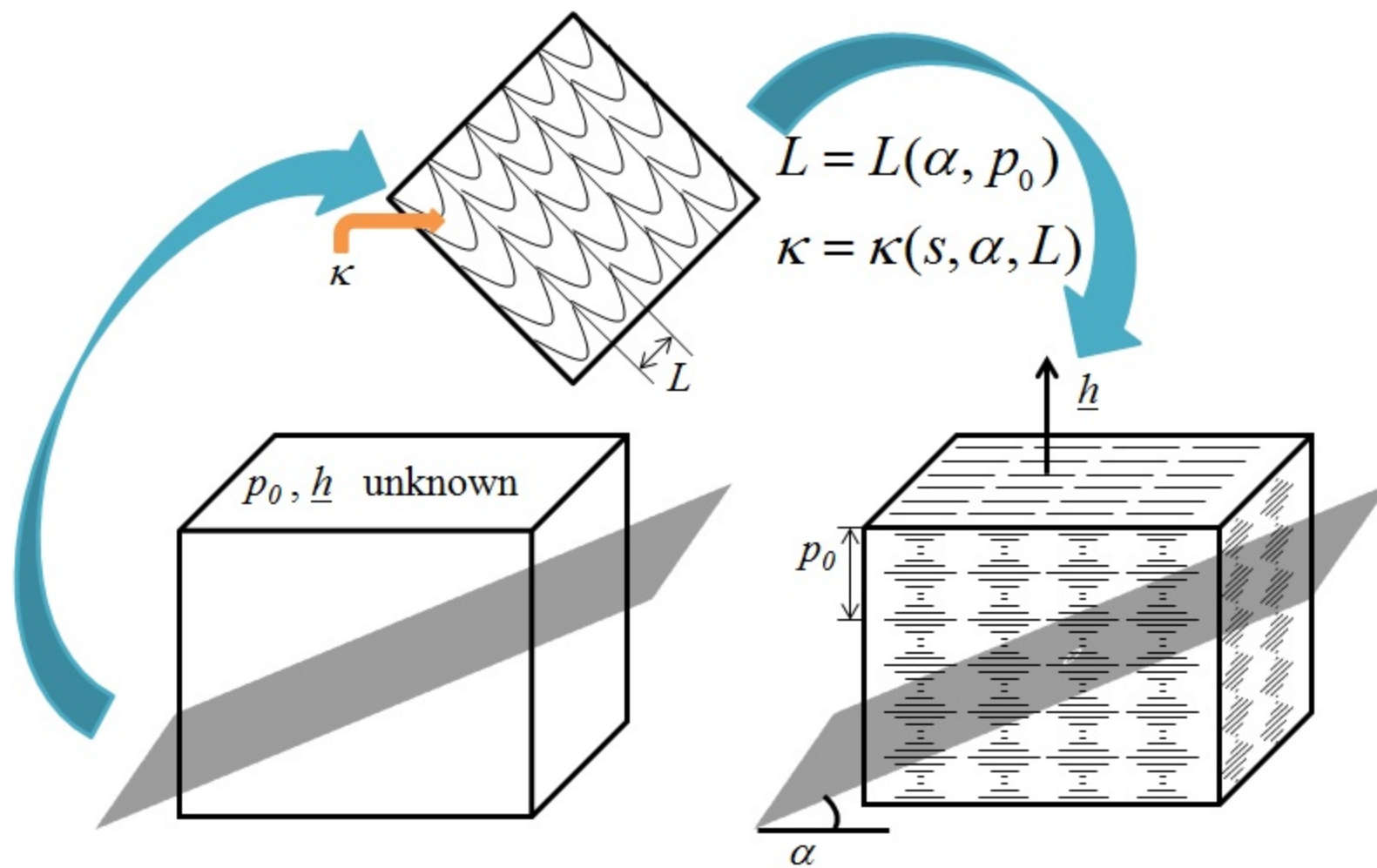


This is an *Accepted Manuscript*, which has been through the Royal Society of Chemistry peer review process and has been accepted for publication.

*Accepted Manuscripts* are published online shortly after acceptance, before technical editing, formatting and proof reading. Using this free service, authors can make their results available to the community, in citable form, before we publish the edited article. We will replace this *Accepted Manuscript* with the edited and formatted *Advance Article* as soon as it is available.

You can find more information about *Accepted Manuscripts* in the [Information for Authors](#).

Please note that technical editing may introduce minor changes to the text and/or graphics, which may alter content. The journal's standard [Terms & Conditions](#) and the [Ethical guidelines](#) still apply. In no event shall the Royal Society of Chemistry be held responsible for any errors or omissions in this *Accepted Manuscript* or any consequences arising from the use of any information it contains.



Cite this: DOI: 10.1039/c0xx00000x

www.rsc.org/xxxxxx

ARTICLE

# Structure Characterisation Method for Ideal and Non-Ideal Twisted Plywoods

Oscar F. Aguilar Gutierrez<sup>a</sup> and Alejandro D. Rey<sup>\*a</sup>*Received (in XXX, XXX) Xth XXXXXXXXX 20XX, Accepted Xth XXXXXXXXX 20XX*

DOI: 10.1039/b000000x

The twisted plywood architecture, known as the Bouligand structure, is a ubiquitous biological and synthetic fibrous composite structure, analogous to that of cholesteric liquid crystals. Twisted plywoods can show ideal or non-ideal structures and are formed via equilibrium or non-equilibrium liquid crystal self-assembly processes. A key to the structure characterisation of plywood films is the specification of the local and global helix vector  $\mathbf{h}(\mathbf{x})$  and pitch  $p(\mathbf{x})$  of the cholesteric order. Previous extensive work demonstrated that oblique cuts of the plywood give rise to arc-patterns that depend both on the unknown incision angle  $\alpha$  and the unknown pitch  $p(\mathbf{x})$ , thus making the precise 3D cholesteric reconstruction ambiguous. In this paper we present an efficient method based on geometric modelling and new visualisation software that determines unambiguously the cholesteric pitch under spatially homogeneous and heterogeneous conditions. The method is applied to films that display two-pitch and spatially non-homogenous structures, as sometimes observed under equilibrium and non-equilibrium self-assembly. The method can be extended to other biological materials such that cornea-like, cylindrical, and various cuticle plywoods.

## 1. Introduction

Nature's ability of assembly of complex multiscale architectures with optimized structural and functional properties provides a source of inspiration for creating and designing new materials<sup>1-6</sup>. The ubiquitous material multiscale organization is obtained using different precursor building blocks such as collagen (vertebrates), chitin (molluscs and insects), and cellulose (plants). Common precursor's features in many biological materials are the fibrillar shape and rigidity, which turn out to be essential ingredients for mesophase stability and liquid crystal self-assembly. In addition to fibrillar rigidity, chemical, geometric and electrostatic chirality is a common source of macroscopic chirality as observed in many self-assembled biological materials<sup>5</sup>. Collagen extracted from living tissue can self-assemble into complex architectures in vitro without the intervention of any tissue-specific cells<sup>4</sup>, establishing the deep correspondence between biological materials and liquid crystals. Biological liquid crystals are generally classified into: (i) solid analogues (plant cell walls, bones, fish scales, cornea) (ii) in-vitro biomacromolecular solutions (collagen, DNA), and (iii) in-vivo (silk proteins, membranes)<sup>5,7</sup>. The interaction between liquid crystal physics and biological mesophases is now generating a better understanding of biological self-assembly and biomimetic principles. In this paper we focus on the use of in-vitro precursors for producing solid chiral liquid crystal analogues, also referred as biological plywoods.

Two types of biological plywoods can be distinguished

according to the assembly process. Equilibrium self-assembled plywoods are formed by directed chiral front propagation, where the helix propagates from a supporting layer into the isotropic phase, leaving behind a defect-free cholesteric which can then be cross-linked<sup>8-9</sup>. Non-equilibrium self-assembled plywoods on the other hand, require a sequence and synchronization of several transport processes to create the plywood. Some stages include fluid flow deposition and subsequent solvent evaporation to induce the liquid crystal phase transition to become a solid analogue<sup>10,11</sup>. Numerous observations indicate that in both cases the resulting plywoods can display ideal or non-ideal architectures. In the former the helical configuration is spatially homogeneous with a constant pitch and fixed helix axis throughout the entire domain while non-ideal plywoods display variable pitch and/or helix axis. The equilibrium plywood self-assembly process has been extensively studied<sup>8,9,12-14</sup> and the non-equilibrium process remains unexplored from the theoretical point of view<sup>15</sup> given the complexity of cholesteric interfaces and nematodynamics<sup>16</sup>. One research driver for the non-equilibrium self-assembly process is the relatively shorter times required for the synthesis of plywoods for biomedical and biotechnological applications. The characterization methodology developed in this paper can be used for equilibrium and non-equilibrium processes.

The objective of the present work is to generalize the twisted plywood architecture models first formulated by Bouligand<sup>6,21</sup> and Giraud-Guille and co-workers<sup>17-20,28-31</sup> and to develop a tool for the 3D reconstruction of ideal and non-ideal plywood

Soft Matter Accepted Manuscript

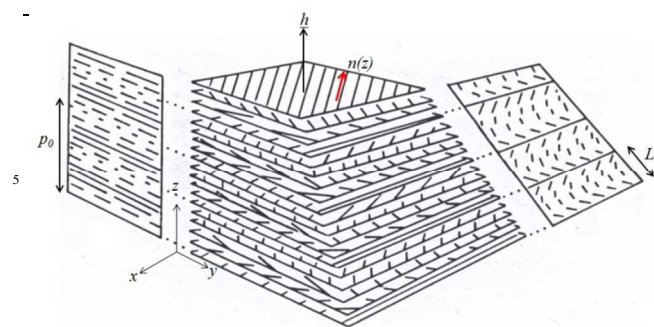


**Fig. 1** Schematic of the twisted plywood architecture, corresponding to a chiral nematic  $N^*$  phase, rectangular coordinates  $(x,y,z)$ . The average molecular orientation or fibrillar units are denoted by the director  $\mathbf{n}(z)$ . The helix axis  $\mathbf{h}=\delta_z$  is normal to the parallel planes, whose distance is half the pitch  $p_0$ . A 2D cross-sectional cut of the 3D plywood results in arced patterns whose periodicity is  $L$ .

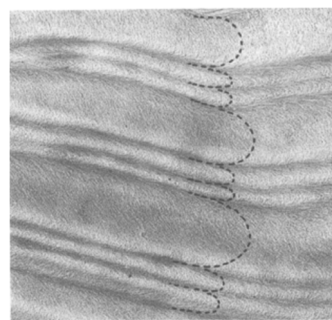


**Fig. 3** (a) Arced pattern for a bimodal (two-pitch) plywood, and (b) arced pattern for ideal single pitch plywood [6]. Copyright permission (3434860436593) from Springer.

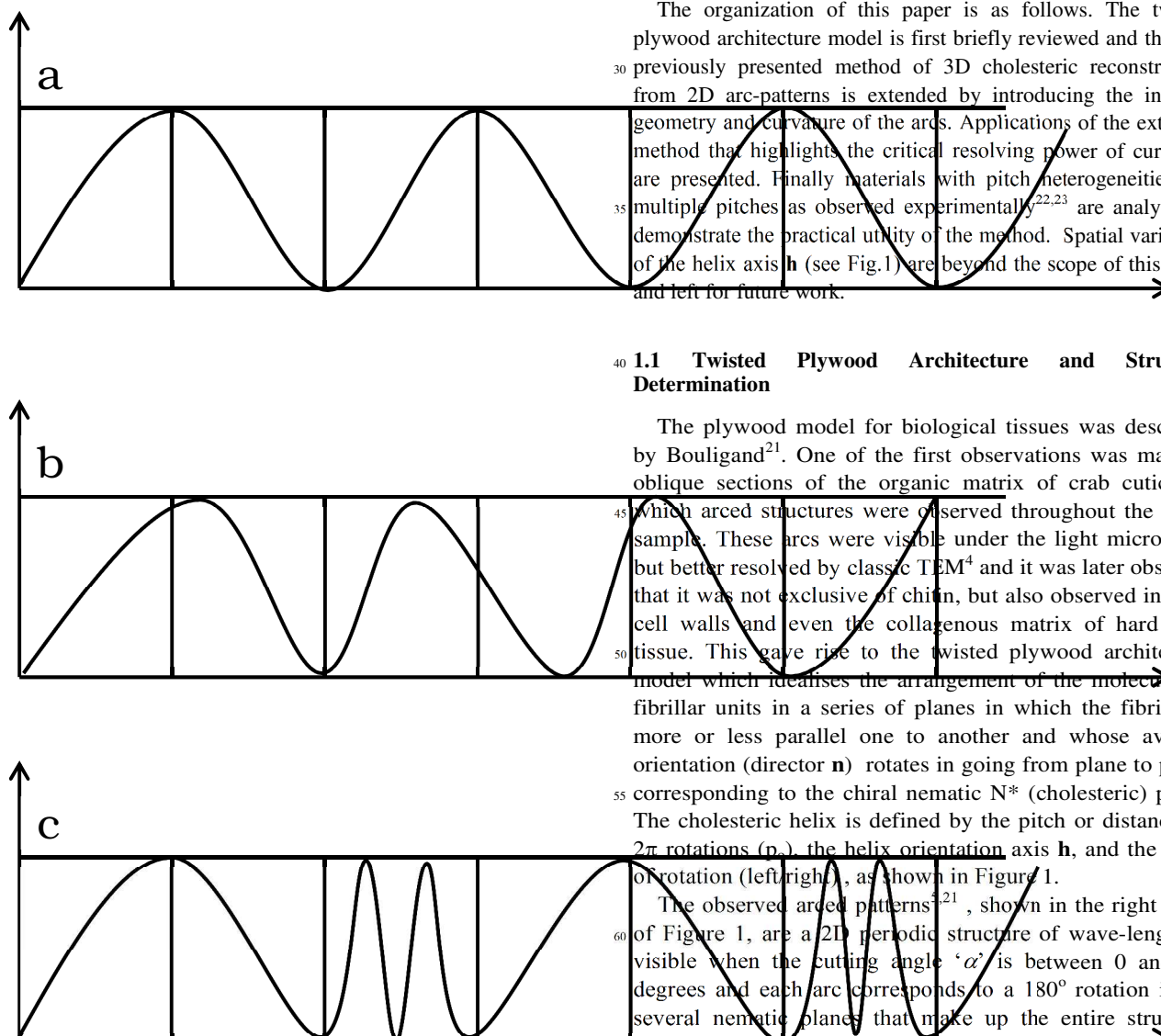


**Fig. 2** Schematic showing a constant periodicity in the microfibril mutual angles (a), non-homogeneous mutual angle leading to a variable periodicity in the arcs (b) and a bimodal pattern that results in a two-pitch plywood (c). Adapted from 22

architectures from typical experimental 2D cross-sectional micrographs.

The organization of this paper is as follows. The twisted plywood architecture model is first briefly reviewed and then the previously presented method of 3D cholesteric reconstruction from 2D arc-patterns is extended by introducing the intrinsic geometry and curvature of the arcs. Applications of the extended method that highlights the critical resolving power of curvature are presented. Finally materials with pitch heterogeneities and multiple pitches as observed experimentally<sup>22,23</sup> are analysed to demonstrate the practical utility of the method. Spatial variations of the helix axis  $\mathbf{h}$  (see Fig.1) are beyond the scope of this paper and left for future work.

### 1.1 Twisted Plywood Architecture and Structure Determination

The plywood model for biological tissues was described by Bouligand<sup>21</sup>. One of the first observations was made in oblique sections of the organic matrix of crab cuticle in which arced structures were observed throughout the entire sample. These arcs were visible under the light microscope but better resolved by classic TEM<sup>4</sup> and it was later observed that it was not exclusive of chitin, but also observed in plant cell walls and even the collagenous matrix of hard bone tissue. This gave rise to the twisted plywood architecture model which idealises the arrangement of the molecules or fibrillar units in a series of planes in which the fibrils are more or less parallel one to another and whose average orientation (director  $\mathbf{n}$ ) rotates in going from plane to plane, corresponding to the chiral nematic  $N^*$  (cholesteric) phase. The cholesteric helix is defined by the pitch or distance for  $2\pi$  rotations ( $p$ ), the helix orientation axis  $\mathbf{h}$ , and the sense of rotation (left/right), as shown in Figure 1.

The observed arced patterns<sup>5,21</sup>, shown in the right panel of Figure 1, are a 2D periodic structure of wave-length  $L$ , visible when the cutting angle ' $\alpha$ ' is between 0 and 90° degrees and each arc corresponds to a 180° rotation in the several nematic planes that make up the entire structure. However when  $180^\circ < \alpha < 360^\circ$  the arcs reverse to their mirror image, which is why the manifestation of these arcs could be thought as the "fingerprint" of supra-molecular chiral structure. Other patterns were identified in bone osteons<sup>17</sup> due to the specific arrangements of collagen fibrils such as the orthogonal plywood architecture and the

cylindrical plywood architecture which can be twisted or orthogonal. The resulting arrangement of at least *in vitro* collagen is a highly pH-dependent process<sup>24,25</sup>; pH  $\approx$  2.5 leads to the twisted plywood architecture but an increase to 3.5 results in the orthogonal plywood<sup>24</sup>.

Later goniometric studies showed that these arcs changed its periodicity  $L$  and when observed at a particular angle these arcs seemed to disappear<sup>22</sup>. This apparent loss of periodicity is an optical effect that was first observed experimentally<sup>20</sup> highlighting the crucial fact that the 2D periodicity “ $L$ ” of the arced patterns is a function of the unknown pitch and unknown incision angle  $\alpha$ :  $L = L(\alpha, p_0)$ , revealing the difficulty to reconstruct the 3D fibrillar chiral organisation from 2D observations.

Structural anomalies can be present due to variations in the relative angle of the fibrils<sup>22</sup>. Some characteristic examples, presented in Figure 2, have been identified in nature<sup>17,22</sup>: (a) ideal architecture ( $p = p_0 = \text{const}$ ) with a constant periodicity, (b) non-uniform pitch ( $p_0 = p_0(z)$ ) and (c) bimodal (two-pitch:  $p_1$  and  $p_2$ ) twisted plywood patterns; examples of (a) and (c) are shown in Figure 3. In the two latter examples  $L$  is not constant since  $L(z) = L(\alpha, p(z))$  and  $L_i = L_i(\alpha, p_i)$ ;  $\{i=1,2\}$ , respectively. It is worth noting that in the case of the two-pitch plywood, the large arc represents only 180° rotation while the smaller arcs a full rotation of the microfibrils is observed. In non-equilibrium self-assembly processes such as the solution casting of collagen

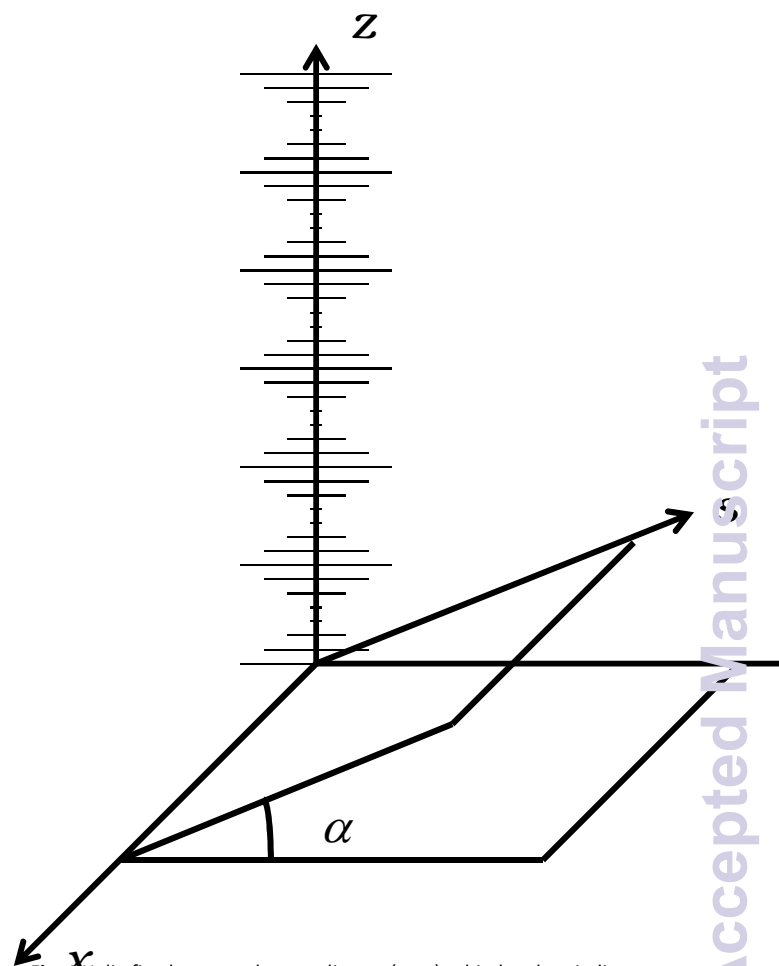


Fig. 4 Helix-fixed rectangular coordinates  $(x, y, z)$ , chiral and periodic cholesteric structure, and incision plane ( $x$ - $s$ ) with an angle  $\alpha$ . The short lines segments normal to the  $z$  axis represent the helical rotation of the macromolecules or fibrils about the helix  $z$ -axis.

films<sup>10,11,15</sup>, these non-idealities (i.e.  $p(z), p_i$ ;  $\{i=1,2\}$ ) will arise from non-homogenous flow-kinematics and/or from uneven solvent evaporation<sup>10,15</sup> or even other process conditions such as pH<sup>24,25</sup>, however the mechanisms remain poorly understood.

As revealed by Figures 1,2 and the fact that the 2D periodicity contains complex information (for example,  $L(z) = L(\alpha, p(z))$  and  $L_i = L_i(\alpha, p_i)$ ;  $\{i=1,2\}$ ), the reconstruction of the 3D plywood organization from 2D micrographs is not a trivial task for either ideal or non-ideal plywoods, and as shown below it requires closer examination of the arcs themselves.

## 2. Geometric Model

### 2.1 Ideal Plywood Model

The geometric model used to describe the twisted plywood is similar to that reported by Bouligand<sup>21,26</sup>, in which a coordinate system is chosen such that the fibrils are parallel to a unit helix vector  $\mathbf{n}$  that rotates about the perpendicular coordinate ‘ $z$ ’ along the helix vector  $\mathbf{h}$ , as

shown in Figure 4. This director field  $\mathbf{n}$  that describes a cholesteric phase is parameterized by the twist angle  $\varphi(z)$ :

$$\mathbf{n} = (n_x, n_y, n_z) = (\cos \varphi, \sin \varphi, 0); \varphi = \frac{2\pi z}{p_0} \quad (1a,b)$$

In Eqn. (1) the pitch “ $p_0$ ” is of the order of 10  $\mu\text{m}$ . As per Eqn.(1b), for ideal plywoods there is a linear relationship between the spatial coordinate ‘ $z$ ’ and the twist angle ‘ $\varphi$ ’.

Taking an oblique cut at an angle  $\alpha$ , shown in Figure 4, defines the incision plane ( $x - s$ ), where  $s$  is the in-plane spatial coordinate whose orientation depends on  $\alpha$ . The projection of  $\mathbf{n}(z)$  to the ( $s$ - $x$ ) plane is the planar vector field  $\mathbf{u}(\alpha, s)$ :

$$\mathbf{u}(\alpha, s) = \left( \cos \left[ \frac{2\pi(\sin \alpha)s}{p_0} \right], \cos(\alpha) \sin \left[ \frac{2\pi(\sin \alpha)s}{p_0} \right], 0 \right) \quad (2)$$

The streamlines  $x = x(s)$  of  $\mathbf{u}(\alpha, s)$  are the experimentally observed 2D arced patterns given by the solution of:

$$\frac{dx}{ds} = \frac{\cot \left[ \frac{2\pi(\sin \alpha)s}{p_0} \right]}{\cos \alpha} \quad (3)$$

Using the boundary condition  $x(0) = x_0$ , the space curve  $x(s, \{\alpha, p_0\})$ , given first by Bouligand, is:

$$x(s, \{\alpha, p_0\}) = x_0 + \frac{p_0}{2\pi \sin \alpha \cos \alpha} \ln \left| \sin \left( 2\pi(\sin \alpha) \frac{s}{p_0} \right) \right| \quad (4)$$

where  $x_0$  is a constant that defines the location of each arc in the  $x - s$  plane and Eqn.(4) describes the trajectories followed by the arced patterns structure and is a periodic function as anticipated; to obtain the 1D periodicity we equate the argument of the logarithmic term to zero and solve for  $s$ . From the first non-trivial solution to the resulting equation, a linear relationship between the periodicity of the structure  $L$  and the pitch  $p_0$  can be extracted:

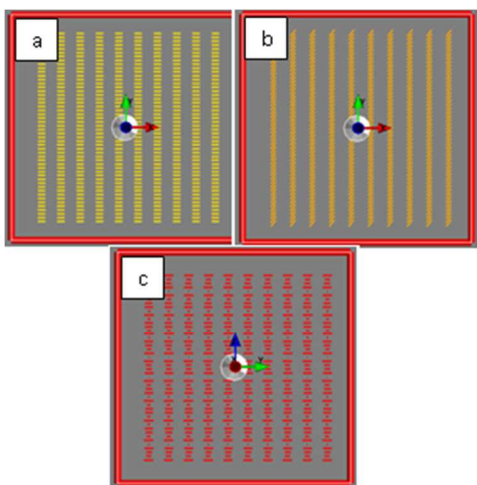


**Fig.5** Computational visualisations of a twisted plywood architecture with no arc-patterns, for  $\alpha = 0^\circ$  (a,b) and  $\alpha = 90^\circ$  (c). For more details see ESI.

$$L = \frac{p_0}{2 \sin \alpha} \quad (5)$$

We emphasize that  $L$  depends on the pitch  $p_0$  and the incision angle  $\alpha$ . This relationship of  $L$  and  $p_0$  can be used for characterisation purposes restricted to knowing  $p_0$  or  $\alpha$ . To remove this degree of freedom or uncertainty, since neither the pitch nor the incision angle is known a priori, we use the curvature  $\kappa(s, \alpha, L)$  of the arced patterns:

$$\kappa(s, \alpha, L) = \frac{-\text{csc}^2 \left( \frac{\pi s}{L} \right)}{\cos \alpha \left\{ 1 + \left( \cot \left( \frac{\pi s}{L} \right) / \cos \alpha \right)^2 \right\}^{3/2}} \quad (6-a)$$

It is worth noting that the maximum curvature depends only on the incision angle:

$$\kappa_{\max} = \frac{1}{\cos \alpha} \quad (6-b)$$

The proposed extended Bouligand model<sup>21,26</sup> for ideal plywoods then is:

$$\text{Ideal Plywood Structure: } \left\{ \begin{array}{l} x(s, \{x_0, \alpha, p_0\}) \\ \kappa(s, \alpha, L) \end{array} \right\} \quad (7)$$

The arced patterns given by Eqn. (4) depend on three parameters:  $x = x(s, \{x_0, \alpha, p_0\})$ . The two important limiting cases not resolved by the analytical model are:  $\alpha = 0, \pi/2$ . In the former case no arced patterns emerge because the cut is taken exactly in any of the  $x$ - $y$  plane of the cholesteric structure, and apparently what would be observed is one of the nematic planes of the whole structure, i.e. an infinite arc represents a straight line parallel to the orientation of the fibrils at any of these nematic planes.

In the latter case no arced patterns can be identified, however the typical cholesteric representation is observed and the periodicity of the structure is  $L = p_0/2$ . To overcome these analytical restrictions and to obtain quick 2D patterns and hence 3D reconstructions for any cutting angle  $\alpha$ , we developed computational visualization software (see supplement for information on implementation of the Mayavi visualization software).

## 2.2 Non-ideal Plywood Model

For non-uniform pitch ( $L(x) = L(\alpha, p(z))$ ) or multiple pitch structures ( $L_i = L_i(\alpha, p_i); \{i=1,2\}$ ), an extended methodology must be applied. Instead of considering a linear relationship between the ‘ $z$ ’ coordinate and the twist angle ‘ $\varphi$ ’ (see Eqn.(1b)), the following twist angles are introduced for the two-pitch and non-uniform plywoods, respectively:

$$\begin{aligned} \varphi = & \frac{2\pi z}{p_0} \left[ H(z) - H\left(z - \frac{p_0}{2}\right) \right] + \\ & \left( \frac{4\pi z}{p_0} - \pi \right) \left[ H\left(z - \frac{p_0}{2}\right) - H(z - p_0) \right] + \\ & \left( \frac{2\pi z}{p_0} + \pi \right) \left[ H(z - p_0) - H\left(z - \frac{3p_0}{2}\right) \right] + \dots \end{aligned} \quad (8)$$

$$\begin{aligned} \varphi = & \frac{2\pi z}{p_0} \left[ H(z) - H\left(z - \frac{p_0}{2}\right) \right] + \\ & \left( \frac{4\pi z}{p_0} - \pi \right) \left[ H\left(z - \frac{p_0}{2}\right) - H\left(z - \frac{3p_0}{4}\right) \right] + \\ & \left( \frac{8\pi z}{p_0} - 4\pi \right) \left[ H\left(z - \frac{3p_0}{4}\right) - H\left(z - \frac{7p_0}{8}\right) \right] + \dots \end{aligned} \quad (9)$$

Where  $H(z)$  is the Heaviside step function. In both expressions the slope is periodic with regular domain lengths of  $p_0/2$  for the two-pitch plywood and irregular domains decreasing periodically for the latter. By modifying Eqn. (1) with Eqns. (8-9) the following general equation is to be solved for each particular non-ideal case:

$$\frac{dx}{ds} = \frac{\cot \{f[H(z, \alpha)]\}}{\cos \alpha}, x(0) = x_0 \quad (10)$$

Where  $f[H(z, \alpha)]$  corresponds to Eqns. (8-9) in terms of 's' and ' $\alpha$ '. The corresponding curvature  $\kappa$  is:

$$\kappa = \frac{-\csc \{f[H(s, \alpha)]\} \frac{df[H(s, \alpha)]}{ds}}{\left( 1 + \left\{ \frac{\cot \{f[H(s, \alpha)]\}}{\cos \alpha} \right\}^2 \right)^{3/2}} \quad (11)$$

For a given incision angle  $\alpha$  the 2D periodicity  $L$  is not a constant throughout the entire structure because  $p_0 = p_0(z)$ ; such expression is particular to each non-ideal plywood and can be periodic as in the case of the two-pitch plywood but also can be monotonous as in the case of the non-homogeneous pitch plywood. To have a modelling closure for these plywoods, the spatial variations of the periodicity can be obtained

experimentally. This leads to a generalized scheme for non-ideal plywoods in terms of space curve ( $x(s)$ ), curvature ( $\kappa$ ) and 2D periodicity ( $L$ ):

$$\text{Non-ideal Plywood Structure: } \left\{ \begin{array}{l} x(s, \{x_0, \alpha, p_0(s)\}) \\ \kappa(s, \alpha, L) \\ L = L(s, \alpha, p_0(s)) \end{array} \right\} \quad (12)$$

### 3. Results and Discussion

#### 3.1 Ideal Constant Pitch Plywoods

Figure 5 (a, b) shows two nematic planes corresponding  $\alpha = 0^\circ$  and Figure 5 (c) shows the typical cholesteric structure corresponding  $\alpha = 90^\circ$ , obtained using the computational visualization software. When  $\alpha$  is close to zero, wide arcs start to appear, which narrow as the angle increases and approaches  $90^\circ$ . For a given  $\alpha$ , the arcs widen as the pitch increases. This leads to the possibility of having two different 3D cholesteric structures with the same 2D periodic structure, which could lead to a wrong characterisation. This uncertainty is demonstrated in Figure 6. Figure 6 (a, c, and d) show the effect on the periodicity  $L$  as  $\alpha$  increases with a constant pitch and figure 6 (a, b) when the pitch increases at constant  $\alpha$ . Hence it is indeed possible to find:

$$L_1 = L_2 \Leftrightarrow p_{0,1} / \sin \alpha_1 = p_{0,2} / \sin \alpha_2 \quad (11)$$

Figure 7 shows the 2D periodicity  $L$  as a function of the pitch  $p_0$  for several  $\alpha$ 's, calculated from Eqn. (5). Increasing  $p_0$  has a stronger effect at smaller  $\alpha$ 's; a horizontal L-constant line proves Eqn. (11).

Another notable case arises when two different incision planes are taken from the same plywood; the first cut being at an angle  $\alpha < 90^\circ$  and the second at the supplementary angle  $\pi - \alpha$ . This is shown in Figure 8 where the arcs have the same periodicity  $L$  however the direction of the arcs are reversed. This orientation

Cite this: DOI: 10.1039/c0xx00000x

www.rsc.org/xxxxxx

ARTICLE

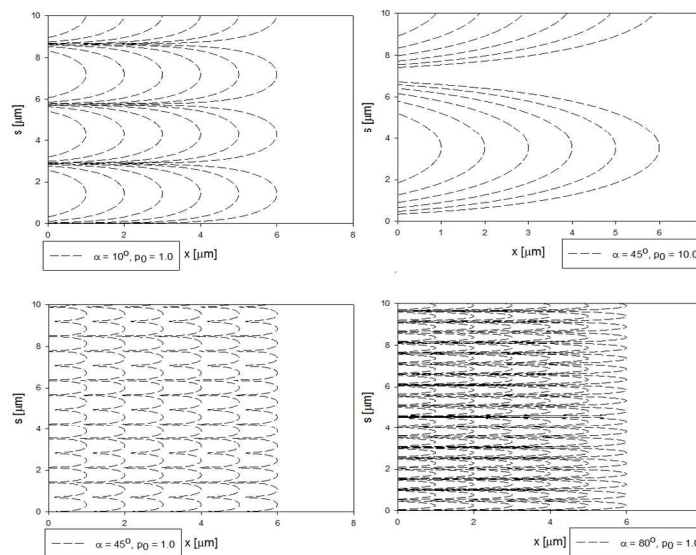


**Fig. 6** Arc patterns of ideal plywoods for increasing incision angle at constant pitch (a, c, and d) and arc patterns for increasing pitch at constant incision angle (b, c).

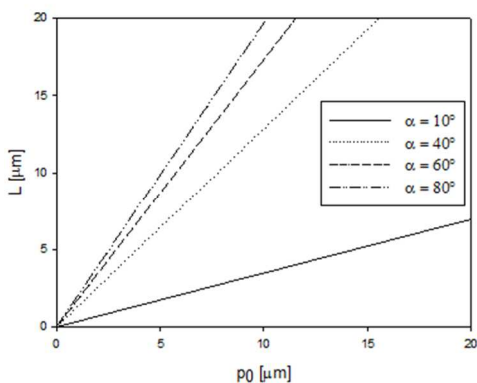


**Fig. 7** Arc periodicity  $L$  as a function of the pitch ( $p_0$ ) for several incision angles ( $\alpha$ ) for ideal plywoods. The increase of  $L$  with  $p_0$  increases with  $\alpha$ .

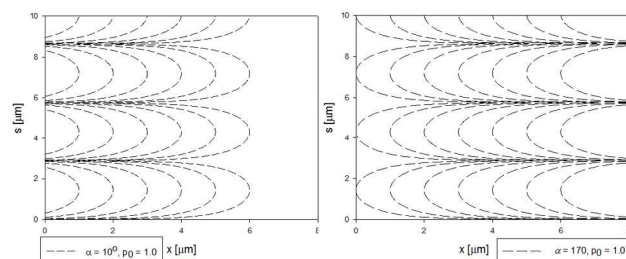


**Fig. 8** Arc patterns of a single ideal plywood obtained from (a)  $\alpha = 10^\circ$  and (b)  $\alpha = 170^\circ$ . The arcs are mirror images because the cutting angle complements.

behaviour had already been observed experimentally where goniometric observations were carried out on fixed samples<sup>15</sup> (constant incision angle) but when tilting the sample in the goniometric stage the arcs cancelled out at a particular angle and the inverse arcs were obtained by further increase in the tilting angle<sup>22</sup>. In Figure 8 the incision angle is not constant and the image reversal is observed because the cutting angle's<sup>20</sup> complementarily.

### 3.2 Non-ideal Plywoods

(a) *Two-pitch plywood* (Eqns.(8-10,12)). Figures 9 and 10 show the twist angle  $\varphi(z)$  profile and arced patterns  $s(x)$ , for a two-pitch plywood. The twist angle  $\varphi(z)$  is constant in each domain of length  $p_0$ , but it oscillates from domain to domain. The smaller (larger) slope corresponds to wider (narrower) arcs. This results replicates Figure 3a.

(b) *Non-homogenous plywood* (Eqns.(9-10,12)). Figures 10 and 11 show the twist angle  $\varphi(z)$  profile and arced patterns  $s(x)$  for a non-homogenous plywood. The twist angle has a constant slope in each domain but it increases from domain to domain. In addition the domain length also decreases. The corresponding arced pattern periodicity  $L$  decreases with “ $s$ ”.

### 3.3 3D Structure Reconstruction Procedure

In order to rebuild the true cholesteric 3D structure by simply using 2D images from experimental micrographs, the curvature  $\kappa(s, \alpha, L)$  of the arcs is introduced as per Eqn.(6-a).

The 3D reconstruction procedure consists of:

- (a) fit of the experimental curvature  $\kappa$  with the eq. (6-a) and obtain  $\alpha$ ;

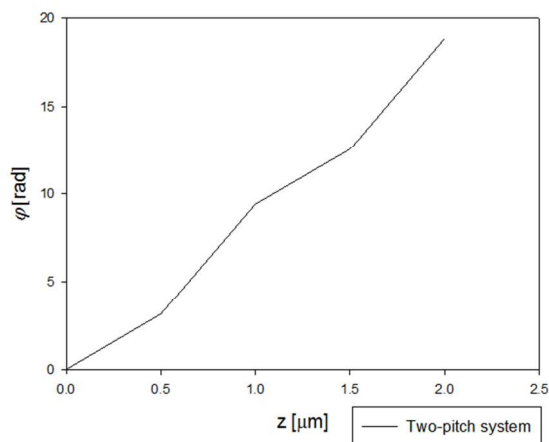


**Fig. 9** Twist angle  $\varphi$  as a function of the spatial coordinate  $z$  for a bimodal (two-pitch) plywood. The slope oscillates from domain to domain. The domain length is constant.

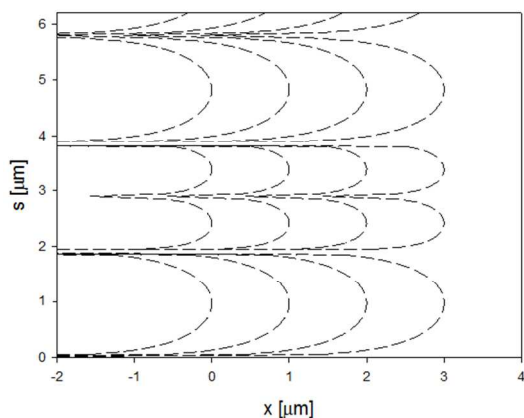


**Fig.10** Arced patterns for the two-pitch plywood, corresponding to Fig.9. The results replicate those of Fig.3a.

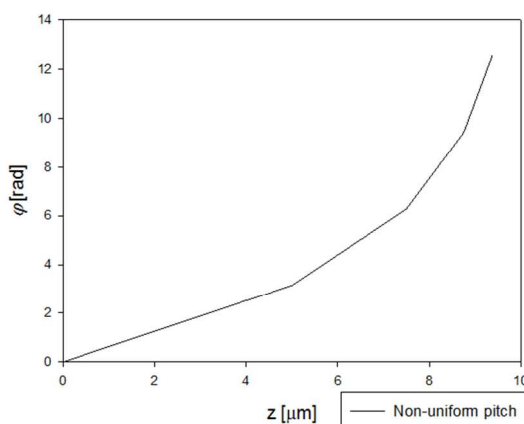


**Fig. 11** Twist angle as a function  $\varphi$  of the spatial coordinate  $z$  for a representative non-uniform pitch. The slope increases from domain to domain. The domain length decreases with  $z$ .

- (b) measure the experimental 2D periodicity  $L$ ;  
(c) solve equation (5) to find the pitch  $p_0$ .

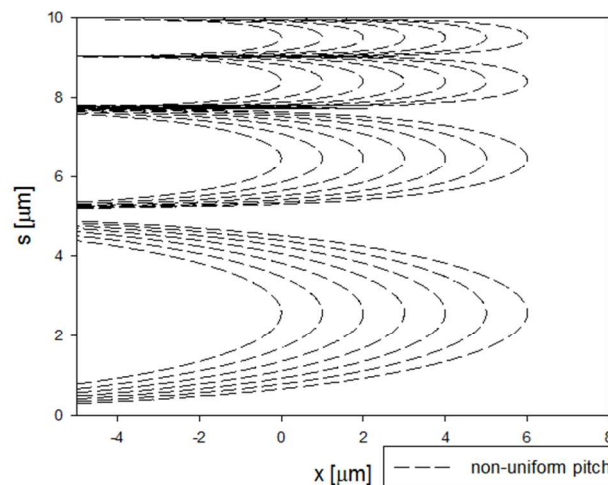


**Fig. 12** Arced patterns  $s(x)$  corresponding to a twist angle given in Fig.11.

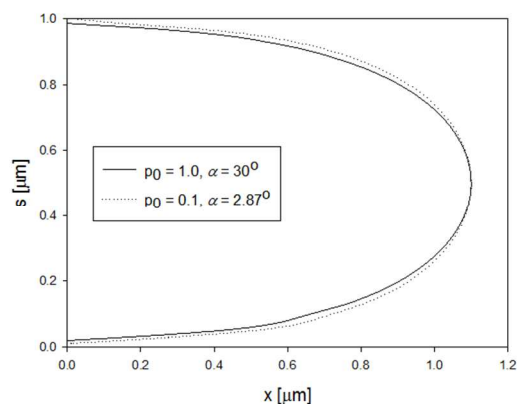
Next we show a representative example to demonstrate the reconstruction capacity of the proposed new procedure (Eqns. (4-7)) using two plywoods with pitches differing by an order of magnitude ( $p_{0,1} = 10p_{0,2}$ ) but showing the same 2D periodicity ( $L_1 = L_2$ ). Figure 13 shows one arc for  $p_{0,1} = 1.0$ ,  $\alpha = 30^\circ$  and another for  $p_{0,2} = 0.1$ ,  $\alpha = 3^\circ$ . The arcs are nearly indistinguishable, correspond to drastically different plywoods, but are made to appear identical by the experimental sectioning. These two plywoods are properly identified when plotting the curvature  $\kappa(s)$  computed from Eqn. (6) as it is shown in Figure 14. The maximum curvature difference is about 15%. It is clear that if the curvature of the arcs is ignored, incorrect predictions can be extracted from the model. This proposed analytical-computational procedure shows significant advantages over the classical pitch determinations which rely on optical measurements that are sometimes restricted to certain pitch ranges<sup>27</sup>. The procedure is applicable to both: equilibrium and non-equilibrium self-assembly plywood formation processes. For plywoods presenting anomalies, as shown with Eqns. (10-12), we proceed with the local determination of  $L_i$ , as it varies as shown in Figure (E5) (see ESI), in these cases  $\alpha$  is available through any of the visible arcs (Eqn. 6 a-b) and the pitch can be calculated in a piecewise manner in each arc, similarly to the ideal case and by appending all the calculated pitches it is possible to know its spatial variations hence, the gradients of the pitch can be identified by constructing a plot like figures (9) and (11), leading to a fuller characterization of the morphology of the twisted plywood.

#### 4. Conclusions

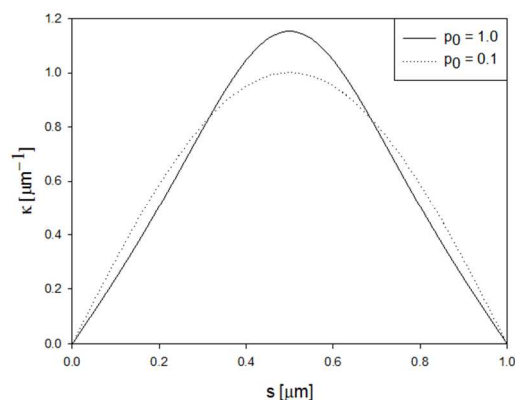
The twisted plywood architecture model originally developed by Bouligand<sup>21,26</sup> was revisited and extended to describe ideal and non-ideal structures arising from pitch gradients and multiple

itches.

A characterisation tool based on analytical results (Eqns.(3-12)) and computational visualization software (see supplement) is



5 **Fig. 13** Comparison between two arcs with the same periodicity and a pitch difference of one order of magnitude.



10 **Fig.14** Curvature  $\kappa$  as a function of spatial coordinate “s” for the two plywoods shown in Fig. 13, with different pitch  $p_0$ , and with the same periodicity  $L$ . The maximum curvature difference between the two cases is about 15% and easily differentiates the two plywoods.

proposed to reconstruct the 3D cholesteric structure of various plywoods from 2D arc-patterns obtained from experimental oblique cuts, which is an alternative procedure to optical measurements of the pitch which may be restricted to certain values of  $p_0$ . A unique and novel feature of our extension is the introduction of curvature and the maximum value of  $\kappa$  (Eqn.6 a-b)) in the observed arcs to eliminate the seldom recognised degree of freedom that exists, since the arcs’ periodicity depend

20 on both the incision angle and the pitch (Eqn.5). This characterisation tool can be used in ideal and non-ideal plywoods (Figs. 6,10,12) by taking into account commonly observed pitch variations in a systematic way (Eqn.(8,9)). Since there is a wide variety in helical arrangements found experimentally (Figs.3), these effective 3D reconstruction computation and visualization tools can be easily extended and applied to any experimental observation of such biological plywoods including the orthogonal cornea-like plywood, the cylindrical plywood configuration, and those found in various

## Acknowledgements

This research was supported by a grant from the Natural Sciences and Engineering Council of Canada. OFAG is grateful for the financial support of CONACyT (Government of Mexico), 35 scholarship number 313480).

## Notes and references

<sup>a</sup> Department of Chemical Engineering, McGill University, Montreal Quebec, H3A 0C5, Canada. E-mail: alejandro.rey @mcgill.ca

† Electronic Supplementary Information (ESI) available: Details on 40 figure 5 and the computational visualisation tool Mayavi. See DOI: 10.1039/b000000x/

- 1 D. Eglin, G. Mosser, M.-M. Giraud-Guille, J. Livage, and T. Coradin, *Soft Matter*, 2005, **1**, 129
- 2 P. Fratzl, *Curr. Opin. Colloid Interface Sci.*, 2003, **8**, 32
- 3 M.M. Giraud-Guille, G. Mosser, C. Helary, D. Eglin, *Micron*, 2005, **36**, 602
- 4 E. Belamie, G. Mosser, F. Gobeaux, M.M. Giraud-Guille, *J. Phys. : Condens. Matter*, 2006, **18**, S115
- 5 A.D. Rey, *Soft Matter*, 2010, **6**, 3402; A. D. Rey, E. E. Herrera-Valencia and Y. Murugesan, *Liquid Crystals*, 2014, 41(3), 430.
- 6 Y. Bouligand, J.P. Denèfle, J.P. Lechaire, and M. Maillard, *Biol. Cell*, 1978, **54**, 143
- 7 A.D. Rey and E. Herrera Valencia, *Biopolymers*, 2012, **97**, 374
- 8 G. de Luca and A.D. Rey, *Physical Review E*, 2004, **69**, 011706
- 9 G. de Luca and A.D. Rey, *Eur. Phys. J.E.*, 2003, **12**, 291
- 10 J.E. Kirkwood and G.G. Fuller, *Langmuir*, 2009, **25**, 3200
- 11 X. Mu and D.G. Gray, *Langmuir*, Article ASAP.
- 12 Y. Murugesan, D. Pasini, A. D. Rey, *Soft Matter*, 2013, **9**, 1054
- 13 Y. Murugesan and A.D. Rey, *Polymers*, 2010, **24**, 766
- 14 A.D. Rey, D. Pasini, Y. Murugesan, *Natural and Biomimetic Materials*, 2011, Y Bar Cohen ed, CRC Press, 131
- 15 G.G. Fuller and J.E. Kirkwood, *USPAP*, US2010/0227043A1
- 16 P. Rofouieeraghi, D. Pasini, A.D. Rey, *Colloid Interface Sci. Commun.*, 2014, **1**, 23; A.D. Rey, *Physical Review E*, 1996, **534**, 4198; A.D. Rey, *Macromolecular Theory and Simulations*, 1995, **45**, 857.
- 17 M.M. Giraud-Guille, *Calcif. Tissue Int.*, 1988, **42**, 167
- 18 L. Besseau, M.M. Giraud-Guille, *J. Mol. Biol.*, 1995, **251**, 197
- 19 F. Livolant, M.M. Giraud-Guille, and Y. Bouligand, *Biol. Cell*, 1972, **31**, 159
- 20 M.M. Giraud-Guille, *Curr. Opin. Solid State Mater. Sci.*, 1998, **3**, 221
- 21 Y. Bouligand, *Tissue Cell*, 1972, **4**, 189
- 22 J.C. Roland, D. Reis, B. Vian, B. Satiat-Jeunemaitre, and M. Mosiniak, *Protoplasma*, 1987, **140**, 75
- 23 S.A. Jewell, P. Vukusic, and N.W. Roberts, *New Journal Phys*, 2007, **9**, 99
- 24 P. De Sa Peixoto, A. Desinet-Besseau, M. Schmutz, A. Anglo, C. Illoul, M.C. Schanne-Klein, and G. Mosser, *Soft Matter*, 2013, **9**, 11241
- 25 F. Gobeaux, E. Belamie, G. Mosser, P. Davidson, P. Panine, and M.M. Giraud-Guille, *Langmuir*, 2007, **23**, 6411
- 26 A. Blumstein, *Liquid Crystalline Order in Polymers*, Academic Press, 1<sup>st</sup> ed, 1978, 261
- 27 H. Baessler and M.M. Labes, *Mol. Cryst. Liq. Cryst.*, 1970, **6**, 419
- 28 M.M. Giraud-Guille, *Tissue Cell*, 1986, **18**, 603
- 29 M.M. Giraud-Guille, *J. Mol. Biol.*, 1992, **224**, 861
- 30 G. Mosser, A. Anglo, C. Helary, Y. Bouligand, M.M. Giraud-Guille, *Matrix Biology*, 2006, **25**, 3
- 31 P. Fratzl and M.M. Giraud-Guille, *Hierarchically Structured Porous Materials: From Nanoscience to Catalysis, Separation, Optics, Energy, and Life Science*. 1<sup>st</sup> ed, 2012, 29